AEM
Journals.ASM.org

Hypothetical Protein Avin_16040 as the S-Layer Protein of *Azotobacter vinelandii* and Its Involvement in Plant Root Surface Attachment

Pauline Woan Ying Liew,[a,b] Bor Chyan Jong,[a] Nazalan Najimudin[b]

Agrotechnology and Bioscience Division, Malaysian Nuclear Agency, Bangi, Kajang, Selangor, Malaysia[a]; School of Biological Sciences, Universiti Sains Malaysia, Minden, Penang, Malaysia[b]

A proteomic analysis of a soil-dwelling, plant growth-promoting *Azotobacter vinelandii* strain showed the presence of a protein encoded by the hypothetical *Avin_16040* gene when the bacterial cells were attached to the *Oryza sativa* root surface. An *Avin_16040* deletion mutant demonstrated reduced cellular adherence to the root surface, surface hydrophobicity, and biofilm formation compared to those of the wild type. By atomic force microscopy (AFM) analysis of the cell surface topography, the deletion mutant displayed a cell surface architectural pattern that was different from that of the wild type. *Escherichia coli* transformed with the wild-type *Avin_16040* gene displayed on its cell surface organized motifs which looked like the S-layer monomers of *A. vinelandii*. The recombinant *E. coli* also demonstrated enhanced adhesion to the root surface.

Azotobacter vinelandii is a Gram-negative free-living and obligate aerobic soil bacterium. It is well known to be a plant growth-promoting bacterium capable of fixing nitrogen and forming desiccation-resistant cysts under unfavorable growth condition (1, 2). The former activity requires it to house several oxygen-sensitive mechanisms while being an obligate aerobic bacterium (3). *A. vinelandii* also has characteristics such as production of plant growth hormones and antibiotics (4) as well as industrially important substances such as extracellular polysaccharide (EPS) alginate, poly-β-hydroxybutyrate (PHB), and siderophore compounds (5).

Many diverse genera of nitrogen-fixing bacteria are present in the plant rhizosphere. The effectiveness of their plant growth-promoting activity depends upon the establishment of their cells in the rhizosphere. This interaction depends upon many factors, one of them being plant exudates. As a diazotroph, *A. vinelandii* provides fixed nitrogen to the plant while acquiring sugars and other nutrients that leak from the roots (6).

The complete *A. vinelandii* genome (GenBank accession number NC_012560) has explained many biochemical pathways and structures of the bacterium (7). It has also revealed hypothetical genes with unannotated functions. The advances in proteomic technology have led to new understanding of and insights into many important proteins and their related mechanisms.

Studies have shown that plant-microbe communication is a two-way interaction involving various signal molecules that cause metabolic changes in both organisms (8–10). Nevertheless, there is limited information on the plant-bacterium interaction, especially with the roots and the rhizosphere. In this study, a proteomic approach was successfully used to study the interaction between a root-associated bacterium and rice plant in the rhizosphere (11–13).

In this study, a differential proteomic analysis of *A. vinelandii* ATCC 12837 in response to different conditions and at different locations within the *Oryza sativa* MR 219 rhizosphere was performed. By two-dimensional gel electrophoresis (2DE) followed by tandem mass spectrometry (MS/MS) analyses, several known and hypothetical proteins were found to be differentially expressed between *A. vinelandii* cells attached to rice root and the planktonic cells. Among these hypothetical proteins, a protein spot putatively identified as Avin_16040 was further studied. The expression of its gene during root surface colonization by *A. vinelandii* was analyzed by quantitative PCR (qPCR). An *Avin_16040* deletion mutant was generated by homologous recombination, and the functional role of Avin_16040 was analyzed by conducting several phenotypic tests, such as a hydrophobicity test, root attachment assay, biofilm assay, and plant growth assay. Supported by bioinformatics information, we attempted to designate an identity for the hitherto-hypothetical protein Avin_16040. The ability to directly compare differential protein expression followed by comparative phenotypic analysis provides the means to identify potentially important proteins in the bacterial response plant-bacterium interaction.

MATERIALS AND METHODS

Bacterial strains, plasmids, and culture conditions. *A. vinelandii* Lipman ATCC 12837 was obtained from the American Type Culture Collection (ATCC), USA. Cultures of *A. vinelandii* was maintained in modified N-free Ashby medium (14). Sucrose 2% (wt/vol) was used as the sole carbon source, and the incubation was performed with continuous agitation at 200 rpm and 26 ± 2°C for up to 5 days. For the comparative proteomic analyses involving plant root-microbe interaction studies, a

Received 25 June 2015 **Accepted** 10 August 2015

Accepted manuscript posted online 14 August 2015

Citation Liew PWY, Jong BC, Najimudin N. 2015. Hypothetical protein Avin_16040 as the S-layer protein of *Azotobacter vinelandii* and its involvement in plant root surface attachment. Appl Environ Microbiol 81:7484–7495. doi:10.1128/AEM.02081-15.

Editor: C. R. Lovell

Address correspondence to Pauline Woan Ying Liew, paulineliew@nuclearmalaysia.gov.my, or Nazalan Najimudin, nazalan@usm.my.

Supplemental material for this article may be found at http://dx.doi.org/10.1128/AEM.02081-15.

modified formulation based on the Murashige-Skoog basal medium with vitamins was used (15). This modified medium (designated AMS+N) consisted of NH_4NO_3 (1.65 g per liter) as the main nitrogen source, while K_2NO_3 was removed. To compensate for the removal of the latter, KH_2PO_4 was also removed, while K_2HPO_4 (522.51 mg per liter), KCl (223.65 mg per liter), and K_2SO_4 (435.67 mg per liter) were introduced. Other supplements in the original Murashige-Skoog basal medium remained the same. The medium was adjusted to pH 5.6. The N-free medium was devoid of NH_4NO_3 and was designated AMS−N. For studies not involving any plant root association, *A. vinelandii* was inoculated into AMS+N and AMS−N to a cell density of 10^6 cells per milliliter and was incubated at 26 ± 2°C for 2 weeks.

For generation of a disrupted mutant using homologous recombination, the kanamycin gene from plasmid pJRD215 was used (16). Plasmid pDM4 was used to assemble the DNA construct containing the disrupted allele (17). For comparative analyses of the *A. vinelandii* mutant and wild-type strains, cells were grown in a modified Burk N-free medium with 2% sucrose as the carbon source (18). Burk+N medium is the modified Burk N-free medium supplemented with 1 g of ammonium acetate, 2 g of tryptone, and 1 g of yeast extract per liter (19).

Competent cells of *Escherichia coli* S17-1λ*pir* and *E. coli* DH5α ECOS 101 were purchased from Yeastern Biotech (Taiwan) and were maintained in Luria-Bertani (LB) medium (Merck, Germany). After transformation with plasmid vector pDM4 (20) or its derivatives, *E. coli* S17-1λ*pir* was grown in Blomfield medium containing the appropriate antibiotics (21) (see Table S1 in the supplemental material). *E. coli* DH5α carrying pJET1.2blunt (Promega, Lithuania) derivatives was maintained in LB medium containing 50 mg liter^{-1} of ampicillin (Sigma-Aldrich, USA). *E. coli* was cultivated overnight at 37°C and 200 rpm.

***Azotobacter vinelandii-Oryza sativa* root association system.** Seeds of *O. sativa* L. cv. MR 219 were dehusked and surface sterilized as previously recommended (22). Sterilized seeds were plated on 0.3% Agar Bacteriological no.1 (Oxoid, United Kingdom) and germinated at room temperature for 2 weeks. Sterile polypropylene containers (100 mm [height] by 55 mm [upper radius] by 40 mm [lower radius]) containing 100 ml of AMS+N or AMS−N were inoculated with fresh *A. vinelandii* ATCC 12837 culture to a final bacterial count of 10^6 CFU ml^{-1}. Eight *O. sativa* MR 219 seedlings were transferred to each container. Plant-microbe association was carried out at 26°C and with 16-h light (40-W light source) and 8-h dark cycles for 2 weeks.

Crude protein extraction and 2DE-MS/MS analysis. The *O. sativa* MR 219 roots with attached *A. vinelandii* ATCC 12837 cells were cropped and shaken vigorously in a lysis solution containing 2% SDS, 0.2% NaOH, 0.05 M EDTA, 2% 2-mercaptoethanol, and Complete protease inhibitor cocktail tablet (Roche, USA) to lyse the bacterial cells. After centrifugation for 15 min at 8,000 × *g* and 4°C, the supernatants containing the bacterial cell lysates were collected. Suspensions of free-floating *A. vinelandii* ATCC 12837 cells unbound to the roots were centrifuged at 8,000 × *g* for 15 min at room temperature before being resuspended in bacterial lysis solution.

Crude proteins were extracted by treating the cell lysates using the standard protocol (23). The protein samples from the root-attached cells involved in plant-microbe interactions in the AMS+N and AMS−N media were designated PM-root(N) and PM-root(0N), respectively. The protein samples from the free-floating cells from the AMS+N and AMS−N media were designated PM-cell(N) and PM-cell(0N), respectively. The proteins from the *A. vinelandii* ATCC 12837 cells not exposed to the plant roots in the AMS+N and AMS−N media were extracted as described for the free-floating cells in the plant-microbe interaction setup, and they were designated CELL(N) and CELL(0N), respectively.

First-dimension processing of crude protein was carried out according to the recommended procedure (Immobiline DryStrip manual) of GE Healthcare (Sweden). Briefly, crude protein pellet (~250 μg) was redissolved up to a volume of 340 μl in rehydration buffer {consisting of 8 M urea, 2% 3-[(3-cholamidopropyl)-dimethylammonio]-1-propanesulfonate (CHAPS), 39 mM dithiothreitol (DTT), 1% Ampholyte 3-10 solution (40%; Sigma-Aldrich, USA), and a trace amount of bromophenol blue in MilliQ processed (18.2 MΩ) water}. Isoelectric focusing (IEF) was conducted with the TV400YK-2D-IEF-SYS horizontal 2DE system (Scie-Plas, United Kingdom) according to the manufacturer's instructions, utilizing a Consort EV232 Power Pac (Scie-Plas, United Kingdom) programmed at 300 V for 1 h, 600 V for 1 h, 1,500 V for 1 h, 3,000 V for 12.5 h, and 300 V for 1 h. The proteins on each gel strip were then reduced and alkylated as described previously (24). For second-dimension gel electrophoresis, the proteins were resolved in 12% SDS-polyacrylamide gels using the Protean II xi system (Bio-Rad, USA) and stained with Coomassie blue according to the manufacturer's instructions. Gel images were captured using the MultiImager II light cabinet (Alpha Innotech, USA). Protein spots of interest were excised from the 2D gel and immersed in 0.1% glacial acetic acid. Sample spots were analyzed by matrix-assisted laser desorption ionization–tandem time of flight (MALDI-TOF/TOF) conducted using the services of a commercial provider (Protein and Proteomics Centre, National University of Singapore, Singapore). The peptide masses (*m/z*) were annotated using Matrix Science's Mascot peptide fingerprinting tools (Table 1) (25). All peptide mass fingerprints were confined to *A. vinelandii* sequence similarities. Semiquantitative evaluation of 2DE protein spot intensity was conducted by ImageMeter 1.1.1 (Flashscript.biz; http://www.flashscript.biz/AIR/imagemeter/ImageMeter.html) (the numeric values in Table 1 show the gel spot intensities).

RT-PCR assay to study expression of the *Avin_16040* gene. Reverse transcription (RT)-PCR was performed to quantify the transcription of the Avin_16040-coding gene. Total RNAs were extracted from the bacterial cells by using the acidic phenol approach (23). The bacterial cells were lysed in lysis solution as described earlier. RNAs were extracted by treating the cell lysates with saturated phenol (pH 4.3), precipitated with cold isopropanol, and dissolved in MilliQ processed (18.2 MΩ) water. The dissolved RNA was quantified and immediately processed for the reverse transcription reaction using the QuantiTect reverse transcription kit (Qiagen, Germany) according to the manufacturer's instructions. The Avin_16040-coding gene was analyzed using custom-designed DNA primers Avin_16040 forward (5′-CTGGCCCTGAGCGACGT-3′) and Avin_16040 reverse (5′-CCACCAGGCGCAGCTTGCCT-3′). The hypervariable V3 region of the 16S rRNA gene was used as the internal control and amplified using DNA primers V3-forward (5′-CCTACGGG AGGCAGCAG-3′) and V3-reverse (5′-ATTACCGCGGCTGCTGG-3′) (13). These primers were designed according to the full genome sequence of the reference strain *A. vinelandii* DJ (accession no. NC_012560). qPCRs was performed using the QuantiFast SYBR green PCR kit (Qiagen, Germany) according to the manufacturer's instructions, with 50 ng of cDNA as the starting template. The reaction was carried out with the CFX96 real-time PCR detection system (Bio-Rad Laboratories, USA). The relative gene expression data were analyzed by the comparative threshold cycle (C_T) method (26).

Construction and validation of the Δ*Avin_16040* deletion mutant. The deletion mutant was constructed by homologous replacement. Three DNA fragments were generated by colony PCR (see Fig. S1 in the supplemental material). These were two DNA fragments located upstream and downstream from the *Avin_16040* gene sequence and a kanamycin resistance (Km^r) gene which was PCR amplified from the pJRD215 plasmid (see Table S1 in the supplemental material). All primers were designed with a restriction enzyme recognition sequence (underlined) at the 5′end as follows: EcoRI-50F (5′-GGGGGGGAATTCTACGGAGTAA CTCCAAGTGA-3′) and SalI-50R (5′-TCAGGCGCATTTCGTCGAC CAACAGACGC-3′) amplified the upstream sequence (701 bp) of *Avin_16040*, XbaI-30F (5′-GCGCGCTCTAGAGGTAGGTGGAGTAG CTGAAGATA-3′) and BamHI-30R (5′-TTTTTTGGATCCAATCCG ATATCCAAATCCGA-3′) amplified the downstream sequence (1,138 bp), and EcoRI-KanF (5′-GGGGGGGAATTCTGGTAAGGTTGGGA AGCCCTG-3′) and BamHI-KanR (5′-TTTTTTGGATCCAGGCGAA CCCCAGAGTCC-3′) amplified the Km^r gene (928 bp). Each fragment was digested with its designated restriction enzyme (New England

TABLE 1 Intracellular peptide analysis results obtained with the Mascot peptide mass fingerprint search tool

Functional group	Protein spot	Mascot match affiliated with *A. vinelandii* DJ	Nominal mass (Da)/pI	Avin gene code	2DE spot intensity[a]					
					CELL (N)	CELL (0N)	PM-cell (N)	PM-cell (0N)	PM-root (N)	PM-root (0N)
Metal ion binding/ transporter	2	gi|226947030, HupE/UreJ protein	15,220/6.92	50400	24	263	2	87	83	511
	6	gi|226947057, molybdenum transporter, periplasmic molybdate-binding protein	26,268/8.45	50670	3	2	7	19	29	99
	9	gi|226942297, periplasmic molybdate-binding protein, ModA2	26,860/7.82	01300	8	16	3	40	6	9
	10	gi|226942297, periplasmic molybdate-binding protein, ModA2	26,860/7.82	01300	8	11	5	27	5	19
	21	gi|226942297, periplasmic molybdate-binding protein, ModA2	26,860/7.82	01300	16	2	3	25	0	7
	23	gi|226947057, molybdenum transporter, periplasmic molybdate-binding protein	26,268/8.45	50670	0	3	7	55	24	26
	26	gi|226947057, molybdenum transporter, periplasmic molybdate-binding protein	26,325/8.45	50670	16	28	26	26	42	133
Structural protein	3	gi|226943338, fimbrial protein	17,010/4.76	12104	0	208	0	1	0	451
	20	gi|226943338, fimbrial protein	17,010/4.76	12104	85	100	210	104	171	153
	63	gi|226944423, major outer membrane porin OprF	37,817/4.44	23330	120	198	6	53	499	447
Oxidoreductase	8	gi|226942238, acid phosphatase/ vanadium-dependent haloperoxidase	27,038/6.54	00690	28	9	20	46	54	54
	27	gi|226942238, acid phosphatase/ vanadium-dependent haloperoxidase	27,038/6.54	00690	2	8	3	11	0	3
	32	gi|226946603, alkyl hydroperoxide reductase	20,879/5.24	45910	191	319	128	104	53	73
Stress response	7	gi|226945904, heat shock protein Hsp20	16,827/5.65	38620	67	88	94	216	146	134
	13	gi|226944659, heat shock Hsp20 protein	22,289/5.00	25770	625	797	363	231	176	99
Molybdenum storage	11	gi|226946344, molybdenum storage protein beta subunit, MosB	27,144/7.82	43210	27	46	48	32	10	18
DNA binding	40	gi|226943301, cold shock domain family protein	7,732/8.09	11700	333	687	1,499	1,138	897	955
Protein folding	12	gi|226944457, phasin protein	20,311/4.93	23670	68	86	57	29	202	95
	35	gi|226944457, phasin protein	20,311/4.93	23670	66	137	26	25	148	143
	38	gi|226944441, peptidylprolyl isomerase	17,820/5.95	23510	26	48	93	91	115	115
	57	gi|226943475, cochaperonin GroES/Cpn10	10,305/5.40	13470	61	46	233	201	245	216
	58	gi|226946146, peptidylprolyl isomerase, FKBP-type	16,973/4.74	41110	50	35	84	34	308	55
	65	gi|226944457, phasin protein	20,311/4.93	23670	316	426	231	310	162	267
Oxygen homeostasis	64	gi|226945828, Fe-superoxide dismutase	21,423/5.14	37820	218	82	85	122	283	354
Electron carrier/ transporter	25	gi|226944991, trimeric LpxA-like superfamily protein	20,175/4.98	29200	67	17	27	32	43	20
	34	gi|226943185, electron transfer flavoprotein beta subunit, FixA	30,878/5.81	10520	277	218	23	4	13	16
	37	gi|226942262, electron transport protein SCO1/SenC	23,120/5.83	00930	272	88	446	486	241	232
	39	gi|226946011, ferredoxin	13,491/6.73	39700	521	1,070	927	1,134	493	1,064
	53	gi|226946011, ferredoxin	13,491/6.73	39700	48	124	370	454	295	287
	59	gi|226946749, thioredoxin 1, Trx1	11,913/4.71	47420	25	59	126	76	46	24
Signal transduction	61	gi|226946071, nucleoside diphosphate kinase	15,465/5.48	40330	136	185	271	258	305	276
Amino acid biosynthesis	15	gi|226942376, tryptophan synthase, alpha chain, TrpA	28,978/5.90	02130	30	14	46	26	9	22
	16	gi|226942376 tryptophan synthase, alpha chain, TrpA	28,978/5.90	02130	33	33	14	5	3	6
	19	gi|226945479, 3-isopropylmalate dehydratase large subunit LeuC	50,937/5.51	34280	13	303	42	297	19	355
ATP synthesis	56	gi|226947192, F_1 sector of membrane-bound ATP synthase, epsilon subunit	15,099/5.19	52150	83	85	57	106	60	62
Posttranslational modification (hydrolase)	22	gi|226942501, peptidase C56, PfpI	20,016/5.80	03390	116	236	148	162	285	312

(Continued on following page)

TABLE 1 (Continued)

Functional group	Protein spot	Mascot match affiliated with *A. vinelandii* DJ	Nominal mass (Da)/pI	Avin gene code	2DE spot intensity[a]					
					CELL (N)	CELL (0N)	PM-cell (N)	PM-cell (0N)	PM-root (N)	PM-root (0N)
Ribonucleoprotein (ribosomal protein)	60	gi|226942915, 50S ribosomal protein L9	15,592/5.09	07670	25	46	13	17	82	96
	62	gi|226942769, 50S ribosomal protein L7/L12	12,524/4.69	06160	342	342	342	342	342	342
Hypothetical protein	1	gi|226943721, hypothetical protein Avin_16040	46,740/4.19	16040	0	53	21	112	1,250	1,172
	4	gi|226946844, hypothetical protein Avin_48400	35,292/7.15	48400	2	1	6	8	0	4
	5	gi|226946844, hypothetical protein Avin_48400	35,292/7.15	48400	2	4	0	4	0	4
	14	gi|226942409, hypothetical protein Avin_02460	44,691/5.80	02460	175	287	143	289	106	263
	17	gi|226945474, hypothetical protein Avin_34230	99,391/4.47	34230	0	23	75	43	22	42
	18	gi|226942972, hypothetical protein Avin_08250	8,341/10.79	08250	171	30	0	15	0	0
	28	gi|226946709, hypothetical protein Avin_47020	11,556/4.90	47020	39	73	73	35	58	34
	54	gi|226947078, hypothetical protein Avin_50890	11,286/6.48	50890	100	215	53	42	49	60

[a] The values presented are 2DE spot intensities according to ImageMeter 1.1.1 software. The protein spots were normalized based on spot 62.

BioLabs, United Kingdom) and fused (1:1:1 concentration ratio) to form a deletion construct of approximately 2.8 kb in size. The deletion construct was then ligated into pDM4 (doubly digested with XbaI and SalI) to form a replacement vector designated pDM4-*16040*m.

Transformation of the replacement vector into *A. vinelandii* ATCC 12837 was performed as previously described, with modifications (18). The bacterium was grown in 10 mM phosphate-buffered Burk medium containing 1% glucose (designated Burk-glucose medium) at 30°C with vigorous shaking (200 rpm) until an optical density at 600 nm (OD_{600}) of ~0.5 was achieved. Subsequently, 1 μg of purified pDM4-*16040*m was added to 50 μl of the bacterial culture. The mixture was incubated at 30°C under static conditions for 2 h, after which it was spread on Burk-glucose agar containing 5 μg ml^{-1} kanamycin. After 2 days of incubation at 30°C, visible colonies on the agar surface were examined for chromosomal integration of the deletion construct. The allelic exchange was confirmed by PCR using custom-designed primers UPSTREAM-50out (5′-TCGACCA GCGAATCCCGTTC-3′) and DOWNSTREAM-30out (5′-TAGAGGTC GTTCGGCTAGATA-3′). The sequences of both primers were not involved in the assembly of the deletion construct and were located outside the recombinational homologous region. The mutant strain should produce a PCR fragment of ~2.9 kb in length, shorter than the expected ~3.3-kb fragment of the wild-type strain.

Phenotypic evaluations of deletion and wild-type strains. (i) Colonial morphology. The colonial morphologies of the *A. vinelandii* ATCC 12837 wild-type and Δ*Avin_16040* mutant strains grown in Burk-sucrose and Burk-sucrose+N agar media were observed. The bacterial strains were streaked and grown for 4 days at 30°C. The size, shape, texture, and color of the bacterial colonies were observed.

(ii) TEM. Thin-section analysis was conducted as recommended previously (27). The wild-type and Δ*Avin_16040* mutant strains were grown in Burk nitrogen-free buffer plus 1% sucrose at 30°C on a rotary shaker at 200 rpm. Transmission electron micrographs (TEM) were captured using a Phillips CM12 scanning transmission electron microscope (Phillips Electron Optics, Netherlands) with a Docu version 3.2 image analysis system (Soft Imaging System GmSH, Germany).

(iii) Biofilm formation assay. The PVC microtiter biofilm screening assay was performed as described previously (28). The wild-type and mutant strains were grown in both Burk-sucrose and Burk-sucrose+N media for 4 days until stationary growth phase was reached (200 rpm, 30°C). The assay was conducted in 5 replications.

(iv) BATH assay. The relative cell surface hydrophobicities of the wild type and the Δ*Avin_16040* mutant were evaluated using the bacterial adherence to hydrocarbons (BATH) assay as reported previously (29). Wild-type and mutant strains were independently cultured in Burk-sucrose and Burk-sucrose+N media at 30°C and shaken at 200 rpm until stationary phase (4 days). The relative cell surface hydrophobicity was determined for the wild type and the Δ*Avin_16040* mutant in both Burk-sucrose and Burk-sucrose+N media. The test was performed in triplicates.

(v) Cell autoaggregation assay. The autoaggregation assay was performed as described previously (30). The wild-type and Δ*Avin_16040* mutant cells were independently grown until stationary phase (4 days) in both Burk-sucrose and Burk-sucrose+N media. The assay was performed in triplicates.

Root attachment assay. The attachments of the *A. vinelandii* ATCC 12837 wild-type and Δ*Avin_16040* mutant strains to the root surface were assayed as described previously (31). *O. sativa* MR 219 seeds were surface sterilized and germinated for 2 weeks with the bacterial cells. Individual roots were cropped and transferred to 1 ml of Burk-sucrose and Burk-sucrose+N media containing 10^6 CFU per ml of wild-type or mutant cells. After 5 days of incubation at room temperature, each root was immersed in 1 ml of sterile 1× phosphate-buffered saline (PBS) solution (Merck, Germany) and vortexed vigorously for 10 s to remove loosely bound bacterial cells. The root was immediately transferred to sterile Whatman paper and air dried for 1 min to eliminate excess water. Subsequently, the root was weighted before being immersed in 1 ml of sterile 1× PBS solution. Root-colonizing bacterial cells were dissociated at 25°C by two sonication pulses (40 kHz) of 1 min each with a pause period of 1 min between the pulses using a Bransonic 5510 ultrasonic bath (Branson, USA). Root colonization was quantified by counting the number of viable cells. The results were normalized to the weight of each root. Each test was carried out in triplicates.

Cloning of the *Avin_16040* gene. The *Avin_16040* gene was amplified by PCR using the primers Avin50 forward (5′-GACCAGCCCGATAGCC TTCG-3′) and Avin30 reverse (5′-GCTGCCCTTTTTCCGCAAGATCA C-3′). Avin50 forward was located at nucleotides 51 to 32 upstream of the start codon, while Avin30 reverse was located at nucleotides 27 to 50

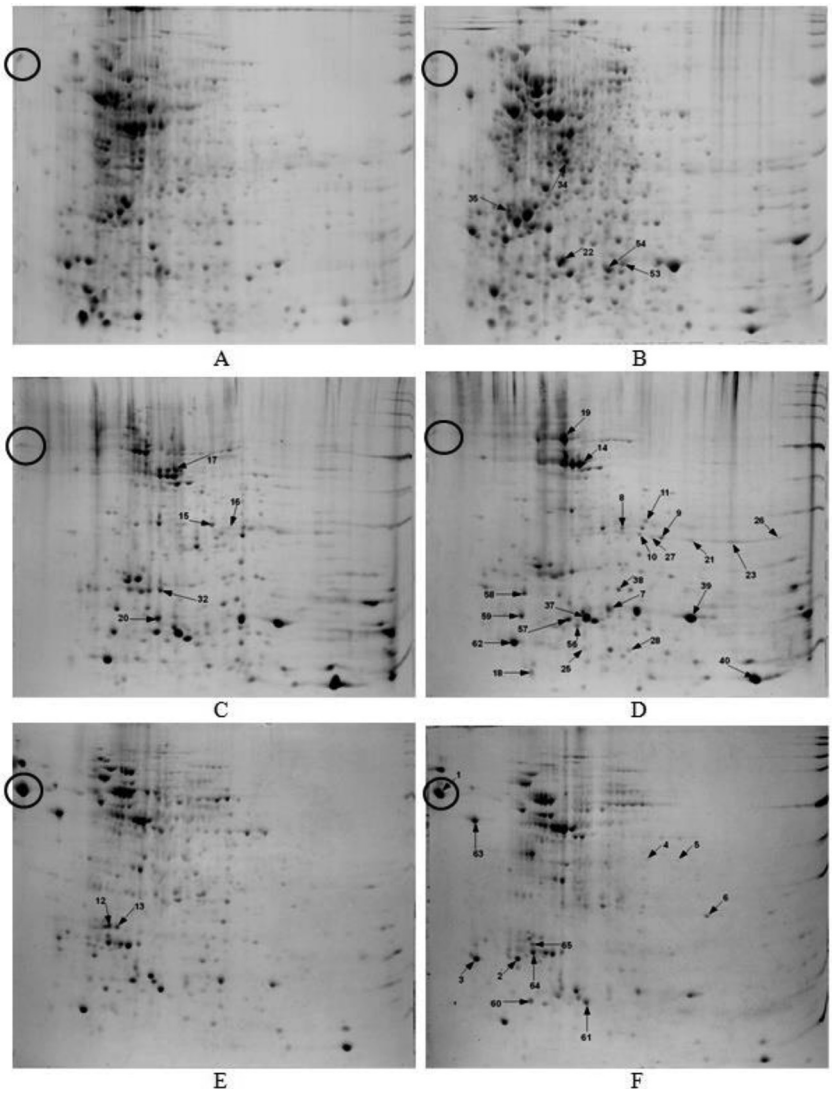

FIG 1 Comparative analysis by 2DE of cell-bound proteomes of *A. vinelandii* ATCC 12837 influenced by different growth conditions. (A) CELL(N); (B) CELL(0N); (C) PM-cell(N); (D) PM-cell(0N); (E) PM-root(N); (F) PM-root(0N). The figure shows the distinctive presence of hypothetical protein Avin_16040 (spot 1, gel location highlighted with black circles) when *A. vinelandii* adhered to the root surface. Arrows indicate 46 protein spots (including spot 1) which showed differential presence under the different growth conditions and spot 62, which was used to normalize the spots' intensity. Detailed information for the protein spots is outlined in Table 1. The protein molecular mass ladder (at right side of each gel) indicates 225, 150, 100, 75, 50, 35, 25, 15, and 10 kDa.

downstream of the stop codon. The amplified PCR product consisting of the open reading frame of *Avin_16040* was cloned into the pJET1.2blunt cloning vector (Fermentas, Lithuania) and transformed into *Escherichia coli* DH5α (ECOS 101 competent cells; Yeastern Biotech, Taiwan). DNA sequencing analysis was performed to obtain the nucleotide sequence of the *Avin_16040* structural gene. DNA sequencing was carried out commercially by Medigene Sdn Bhd. with cloning vector primers.

The freshly cultivated recombinant clone was smeared on a glass slide and air dried. Gram staining was performed as described previously (23). The slide was viewed using a Primo Star upright microscope (Zeiss, USA) at a magnification of ×1,000 with immersion oil. *E. coli* DH5α without plasmid was also cultivated and used for comparison.

Bioinformatic analyses of the *Avin_16040* gene sequence. Gene sequences were analyzed with BLASTN, TBLASTX, and BLASTP (http://blast.ncbi.nlm.nih.gov/, last accessed 15 February 2013). Multiple-sequence alignment was performed with the ClustalW Multiple Alignment program (32). The presence of transmembrane helices was predicted with programs HMMTOP version 2.0 (33) and TMHMM server v. 2.0 (34). To predict the presence of protein translocation machinery, the translated amino acid sequence of Avin_16040 was submitted to the SignalP 4.0 server of the Center for Biological Sequence Analysis (http://www.cbs.dtu.dk/, last accessed 15 February 2013). Subsequently, the amino acid sequence of the *A. vinelandii* Avin_16040 signal peptide was analyzed with the NCBI PSI-BLAST search tool (http://blast.ncbi.nlm.nih.gov/, last accessed 15 February 2013) against the nonredundant protein database to obtain its homology matches.

AFM. Atomic force microscopy (AFM) was conducted using a JPK-NanoWizard II system (JPK Instruments AG, Germany) to analyze the cell surface topography of wild-type *A. vinelandii* ATCC 12837, the Δ*Avin_16040* deletion mutant, and the *E. coli* DH5α transformant containing the Avin_16040-coding gene. Samples were prepared by smearing the bacterial cells onto glass slides before subjecting them to a short fixation period of 45 s in glutaraldehyde (2% in PBS containing Ca^{2+} and Mg^{2+}) followed by an incubation of 20 min in paraformaldehyde (4% in

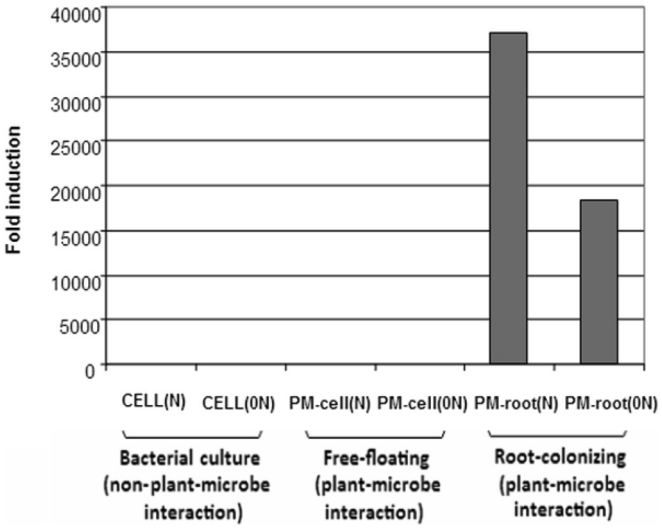

FIG 2 Analysis by RT-PCR of the relative expression levels of *Avin_16040* in *A. vinelandii* ATCC 12837 cultivated under different growth conditions for 2 weeks. The expression of *Avin_16040* was normalized against the 16S rRNA gene. N and 0N represent N-enriched and N-free media, respectively.

PBS containing Ca^{2+} and Mg^{2+}) according to the manufacturer's recommendation.

Nucleotide sequence accession number. The complete sequence of the *Avin_16040* structural gene has been deposited in the NCBI GenBank database under accession number KF049202.

RESULTS

Proteomic analysis. The proteomes of the *A. vinelandii* planktonic and root-attached cells incubated under nitrogen-free and nitrogen-enriched conditions were compared. Overall, 46 cell-bound protein spots were excised from 2D gels (Fig. 1) and identified by MALDI-TOF/TOF peptide mass fingerprinting (Table 1). Among these proteins, 2DE spot 1 (identified as the hypothetical protein Avin_16040), which showed an intense response to root surface attachment (Fig. 1), was further analyzed.

Relative quantification of *Avin_16040* mRNA using qPCR. The expression of the gene was quantified by qPCR (Fig. 2). Bacterial cells that were exposed to rice roots for 2 weeks were used. The *Avin_16040* gene showed high levels of transcripts in the root-attached *A. vinelandii* ATCC 12837 cells relative to those in the free-floating cells. In the nitrogen-enriched medium, the expression was 37,122-fold higher, while in the nitrogen-free medium, it was 18,305-fold higher, compared to 1- and 3-fold, respectively, for the free-floating cells (Fig. 2).

Bioinformatics analyses show that Avin_16040 is similar to a surface layer protein. The DNA sequence of the structural gene of Avin_16040 revealed a complete open reading frame (ORF) of 1,368 bp in length (see Fig. S2 in the supplemental material) that matched the *Avin_16040* gene of *A. vinelandii* DJ (GenBank accession no. NC_012560) with 97% identity (1,327/1,368 nucleotide bases). The predicted ORF of *Avin_16040* for *A. vinelandii* ATCC 12837 was larger than that for *A. vinelandii* DJ by three nucleotides (one codon) (see Fig. S3 in the supplemental material). Its deduced amino acid sequence matched the Avin_16040 protein of *A. vinelandii* DJ with a 97% identity (see Fig. S4 in the supplemental material). A BLASTP analysis against the nonredundant protein database showed that the deduced amino acid sequence of Avin_16040 shared 39% identity with the surface layer protein of *Aeromonas hydrophila* (GenBank accession no. ACV89427), 38% identity with the paracrystalline surface layer protein of *A. hydrophila* (GenBank accession no. AAA67043), and 32% identity with the paracrystalline surface layer protein of *Pseudomonas stutzeri* DSM 4166 (accession no. YP_005940513) (see Fig. S4 in the supplemental material). Multiple-sequence alignment of these amino acid sequences showed highly conserved amino acid sequences at both the N and C termini (see Fig. S5 in the supplemental material). Further, predictions for surface protein transmembrane helices using two independent programs, HMMTOP version 2.0 and TMHMM v. 2.0, predicted a transmembrane helix of 18 amino acids at the N terminus (see Fig. S6 in the supplemental material). The hypothetical protein also contains a putative signal peptide of 20 amino acids (MMKKSLLALA VAALSANAF**A**) which overlapped with the sequence of the predicted transmembrane helix structure. A signal peptidase cleavage site was detected directly after the amino acid alanine (A) (see Fig. S7 in the supplemental material). Using NCBI PSI-BLAST analysis, this predicted signal peptide showed the highest similarity (84%) to the signal peptide of the *P. stutzeri* DSM 4166 paracrystalline surface layer protein (see Table S2 in the supplemental material).

Allelic exchange mutagenesis to generate an *Avin_16040* deletion mutant. PCR fragments of the *Avin_16040* upstream and downstream regions and the interrupting kanamycin gene were successfully amplified and assembled into plasmid pDM4 to produce pDM4-*16040m*. Restriction digestion with XbaI verified a plasmid size of approximately 10 kb (see Fig. S8 in the supplemental material), while double digestion with XbaI and SalI produced two DNA fragments of 2.8 kb and 7 kb, representing the deletion construct and the pDM4 backbone, respectively. An *Avin_16040* deletion mutant was then generated by transforming the replacement vector into *A. vinelandii* ATCC 12837, selecting for kanamycin resistance. Counterselection of *sacB* was achieved on Burk agar containing 10% sucrose to isolate colonies containing a successful double-crossover recombination event. PCR analysis amplified a single DNA band of 2.9 kb in size using the primers UPSTREAM-50out and DOWNSTREAM-30out, in contrast to a PCR band of 3.3 kb in size generated from the wild-type strain. The result verified the allelic replacement of the wild-type *Avin_16040* gene with the deletion allele in the *A. vinelandii* ATCC 12837 genome (see Fig. S9 in the supplemental material). A further validation by 2DE confirmed the deletion, based on the disappearance of the Avin_16040 protein spot from its location on a 2D gel (see Fig. S10 in the supplemental material). The deletion mutant was designated the *A. vinelandii* Δ*Avin_16040* strain.

Phenotypic changes of the Δ*Avin_16040* mutant. (i) Colonial morphology. The mutant colony was whitish opaque in color, compared to the creamy yellow of the wild-type strain (Fig. 3). In addition, the mutant colony showed a unique appearance by having clear zones within it, as if spots of lysis had locally taken place (Fig. 3B, arrows). Both the wild-type and mutant colonies were covered with mucus. However, the mucoidal substance of the mutant appeared more opaque, more watery, and with a softer texture than that of the wild type.

(ii) TEM. Figure 4 shows the thin-section analysis by TEM of the interior structure of the wild-type and Δ*Avin_16040* mutant strains. Both the wild-type and mutant strains showed large granules within the cells, which are suspected to be polyhydroxybu-

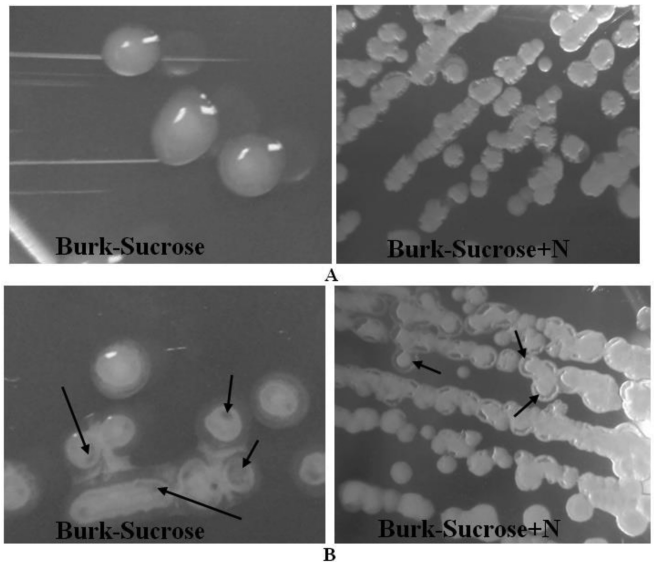

FIG 3 Physical appearance of bacterial colonies of wild-type *A. vinelandii* ATCC 12837 (A) and the Δ*Avin_16040* mutant strain (B) after cultivation for 4 days on Burk-sucrose (N-free) and Burk-sucrose+N agar at 30°C. The mutant displayed a unique appearance with a clear zone of lysis within the colony. The clear zones are indicated by arrows.

tyrate granules. However, the wild-type cell was completely bordered by a well-defined layer of cell membrane (Fig. 4A, arrow), while the mutant cells were only partially bordered (Fig. 4B). At higher magnification, this thick layer surrounding the wild-type bacterial cell resembled the S-layer matrix. This structure was noticeably absent in the mutant.

(iii) Biofilm formation assay. The Δ*Avin_16040* mutant grown in the N-free Burk-sucrose medium demonstrated biofilm formation that was decreased by more than 50% compared to that of the wild type (Fig. 5). However, no significant difference was detected when grown in the N-rich Burk-sucrose+N medium.

(iv) BATH assay. The bacterial cell surface hydrophobicity was estimated based on the ability to bind with hydrocarbon hexane. When the Δ*Avin_16040* mutant was grown in Burk-sucrose medium, the bacterial strain totally lost its cell surface hydrophobicity. In contrast, the wild-type strain demonstrated a hydrophobicity value of 21% (Fig. 6). Both the mutant and wild-type strains showed low levels of hydrophobicity (<5%) when grown in Burk-sucrose+N medium.

(v) Autoaggregation assay. Autoaggregation of the bacterial cells was estimated based on the sedimentation rate of the bacterial cells. Generally, the Δ*Avin_16040* mutant demonstrated significantly reduced autoaggregation when grown in either the Burk-sucrose or Burk-sucrose+N medium. The effect was more evident for the cells grown in the Burk-sucrose+N medium, in which the Δ*Avin_16040* mutant strain showed 18% lower autoaggregation ability than the wild-type strain. The results are shown in Fig. 7.

(vi) Root attachment assay. The root attachment ability of the *Avin_16040* mutant was significantly reduced, by an order of magnitude, compared to that of the wild type when assays were performed in both Burk-sucrose and Burk-sucrose+N media (Fig. 8). Each strain showed an approximately 1-fold-higher root at-

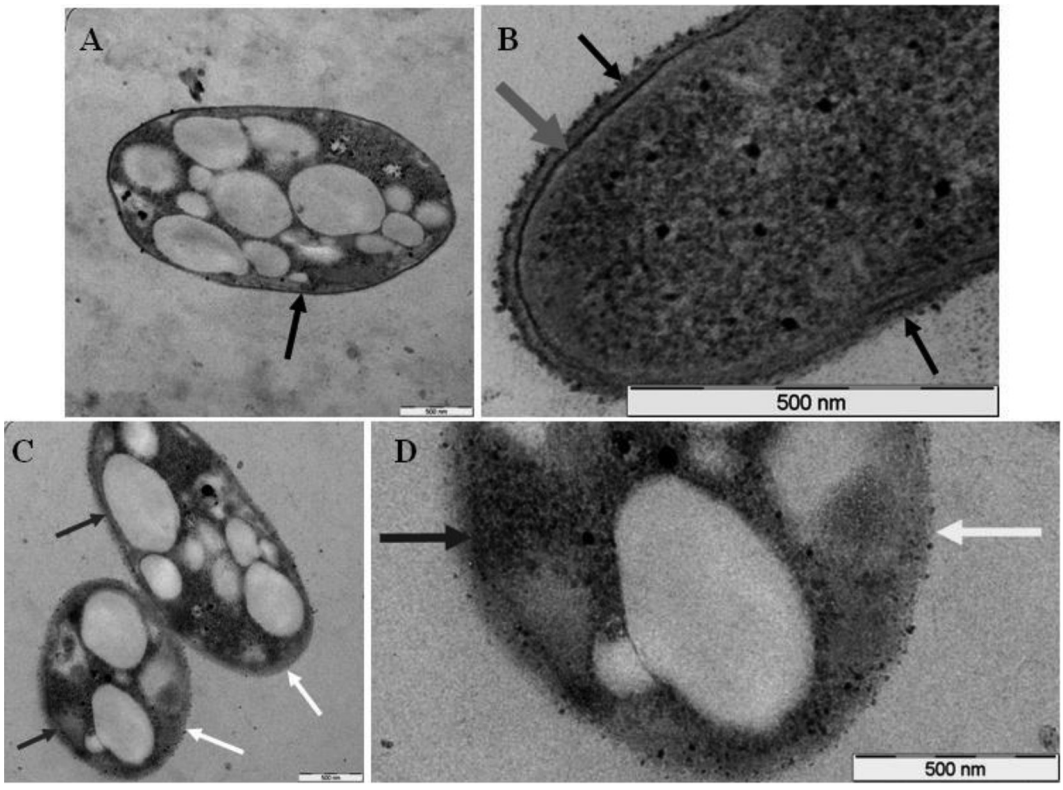

FIG 4 TEM analyses of wild-type *A. vinelandii* ATCC 12837 (A and B) and the Δ*Avin_16040* mutant (C and D). Mutant cells displayed an absence (white arrows) of S-layer matrix available on the wild-type cell surface (black arrows). The dark gray arrows (C and D) and the thick gray arrow (B) indicate the cell membranes.

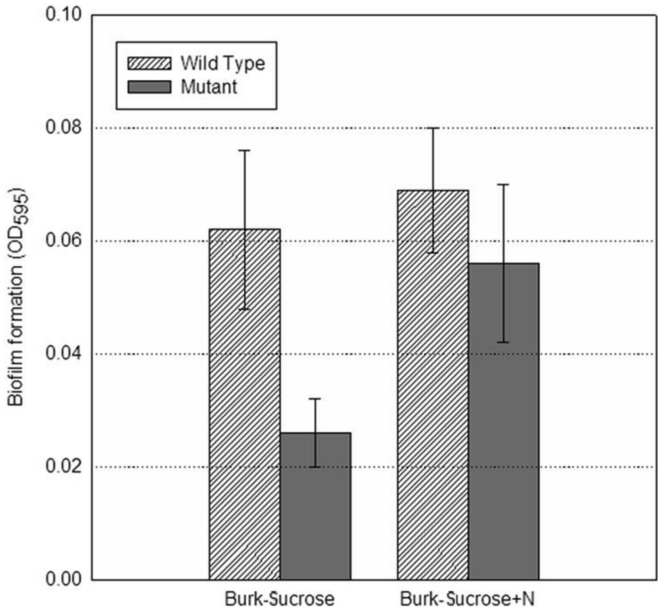

FIG 5 Evaluation of biofilm formation by comparing wild-type and Δ*Avin_16040* mutant strains in Burk-sucrose and Burk-sucrose+N media. The mutant strain showed significantly reduced biofilm formation in Burk-sucrose medium (N free). No significant change in biofilm formation was observed in Burk-sucrose+N medium (N rich).

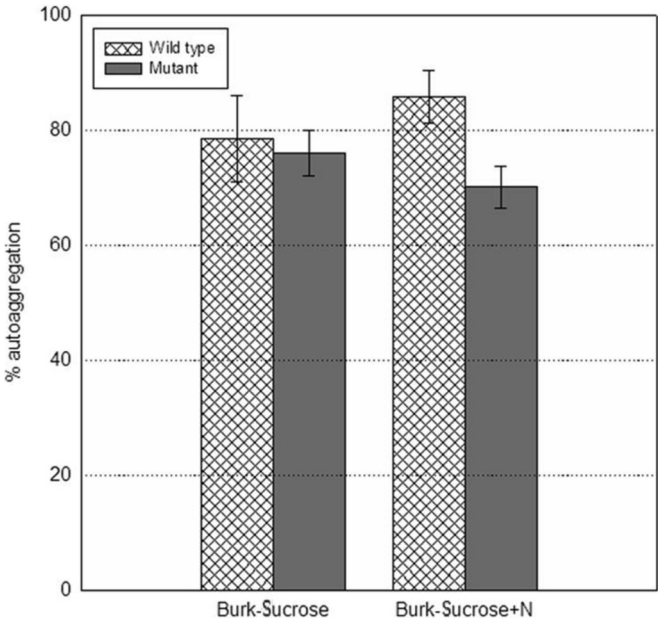

FIG 7 Evaluation of bacterial cell autoaggregation of *A. vinelandii* ATCC 12837 wild-type and Δ*Avin_16040* mutant strains in Burk-sucrose and Burk-sucrose+N media. The Δ*Avin_16040* mutant strain showed reduced autoaggregation compared to that of the wild-type strain.

tachment ability when grown in Burk-sucrose medium (N free) than when grown in Burk-sucrose+N medium (N rich). *E. coli* DH5α cells containing the *Avin_16040* gene showed an enhanced root surface attachment ability compared to that of the negative control which did not contain the gene (Fig. 9).

(vii) Optical microscopy analysis. Figure 10 shows optical microscopic views of bacterial clone *E. coli* DH5α carrying recombinant plasmid pJET1.2blunt ligated with the full gene sequence of *Avin_16040*. When examined by Gram staining, the recombinant clones carrying both insert orientations displayed the same cell morphological change. In comparison to nontransformed *E. coli* DH5α cells, a recombinant clone with pPLN0009 showed elon-

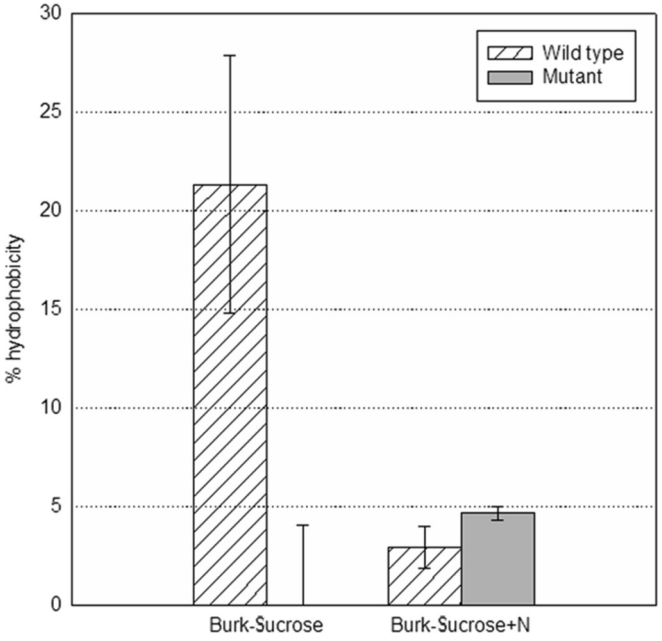

FIG 6 Analysis of cell surface hydrophobicity of *A. vinelandii* ATCC 12837 wild-type and Δ*Avin_16040* mutant strains in Burk-sucrose and Burk-sucrose+N media. The mutant strain lost its cell surface hydrophobicity when grown in the Burk-sucrose medium (N free).

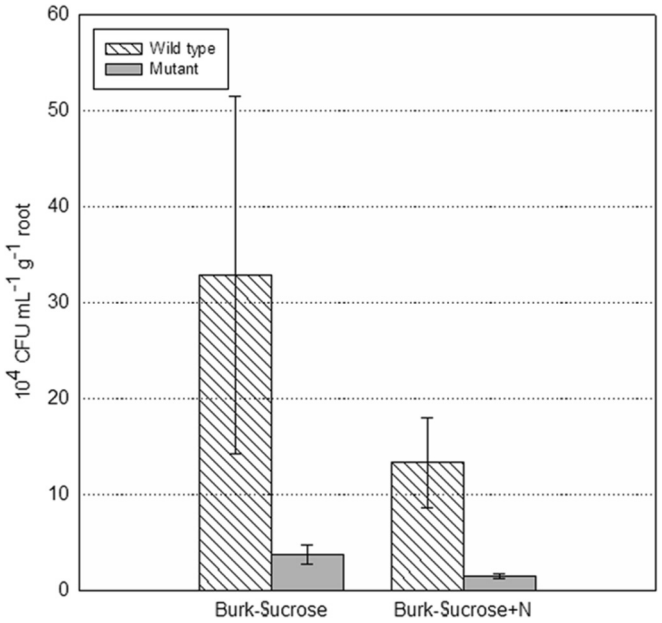

FIG 8 Attachment to the root surface by *A. vinelandii* ATCC 12837 wild-type and Δ*Avin_16040* mutant strains. The mutant strain showed decreased root surface attachment in both Burk-sucrose and Burk-sucrose+N media.

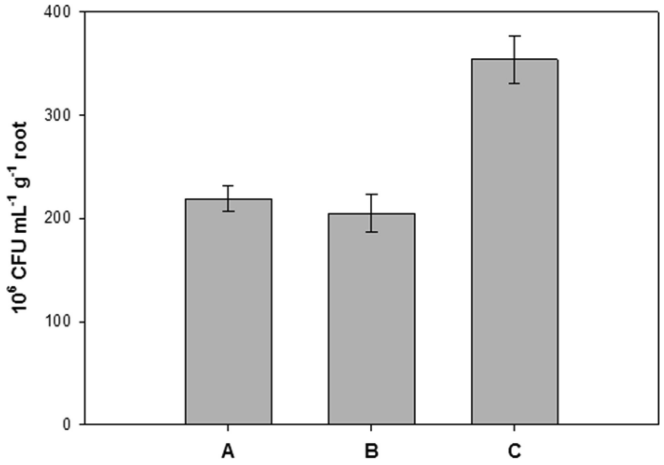

FIG 9 Attachment to the root surface by *E. coli* DH5α(pJET1.2blunt-*Avin_16040*) (C). Negative controls were *E. coli* DH5α containing no plasmid (A) and *E. coli* DH5α(pJET1.2blunt-rDNA) (B). The *E. coli* DH5α(pJET1.2blunt-Avin_16040) recombinant clone showed increased root surface attachment compared to that of the negative controls.

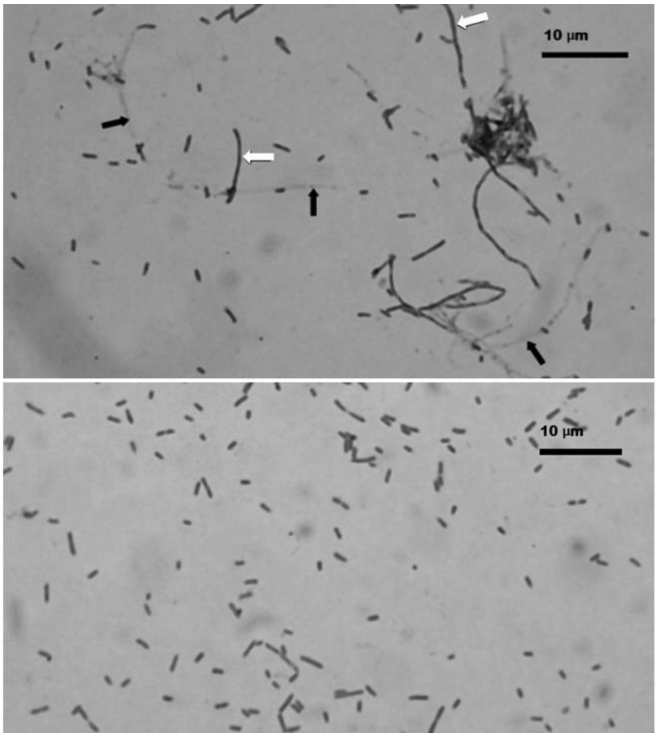

FIG 10 Light microscopic images of the *E. coli* DH5α clone (carrying plasmid pJET1.2/blunt-*Avin_16040*) (upper panel) and transformation host (no plasmid) (lower panel) at a magnification of ×1,000. The white and black arrows indicate the elongated (filamentous) cell and transparent "tube-like" structures, respectively.

gated (filamentous) cell morphology. In addition, transparent "tube-like" structures were also observed, and these were interspersed with single cells.

(viii) AFM analysis. Atomic force microscopy (AFM) analysis revealed different cell surface topographies for the *A. vinelandii* ATCC 12837 wild type and the Δ*Avin_16040* deletion mutant (Fig. 11). The wild-type cell displayed a structure that resembled the S-layer matrix on the surface (Fig. 11A), while the surface of the mutant was smooth (Fig. 11B).

DISCUSSION

Plant-microbe interactions have drawn much attention because of their contribution to plant growth. Root attachment and colonization constitute an important stage, and little is known about their mechanisms. *A. vinelandii* has been known to be a good plant growth-promoting bacterium (2, 4). In this study, the response of *A. vinelandii* to association with the roots of *O. sativa* was examined under different growth medium conditions.

One of the proteins that was present exclusively in root-attached cells was annotated as hypothetical protein Avin_16040 in the *A. vinelandii* DJ genome database. Its occurrence suggested its involvement in the association of *A. vinelandii* and *O. sativa* roots. This protein showed its distinctive presence only when *A. vinelandii* ATCC 12837 was attached to the root surface. The expression of the *Avin_16040* gene was quantified using qPCR, and the result suggested an induction of the *Avin_16040* gene during the root attachment of the bacterial cells.

The Avin_16040 protein in *A. vinelandii* ATCC 12837 was shown to be 97% identical to that in *A. vinelandii* DJ. The deduced amino acid sequence shared 39% identity with the bacterial paracrystalline surface layer (S-layer) protein of *Aeromonas hydrophila* and 32% with that of *Pseudomonas stutzeri* DSM 4166. These bacterial strains were all reported to array their S-layer proteins with a tetragonal symmetry (35–39). This monomolecular layer of crystalline proteinaceous subunits forms one of the most common surface structures on bacteria and archaea (40–44).

The bacterial S-layer protein was predicted to have a transmembrane helix and undergo a posttranslational modification by signal peptide excision (45, 46). The Avin_16040 protein was also predicted to have a transmembrane helix at the N terminus preceded by an overlapping signal peptide of 20 amino acids. Its deduced homology to the paracrystalline surface layer proteins substantiated with the presence of transmembrane helix and signal peptide suggested that Avin_16040 is possibly a surface layer protein. The surface layer (S-layer) protein is usually associated with surface attachment defense mechanism and bacterial signaling functions (38). Typically, it consists of two structural regions in which two essential functions reside. One region is involved in the attachment of the S-layer subunit to the cell envelope (transmembrane region), while the other is involved in assembly (47).

The Avin_16040 expression by root-attached cells indicated possible involvement of this protein with root surface attachment. According to Merrigan et al. (48), bacterial surface protein is one of the bacterial cell surface attachment elements. The role of bacterial surface protein as a surface adhesin matched the expression behavior of Avin_16040. Subsequently, an *Avin_16040* deletion mutant, designated *A. vinelandii* Δ*Avin_16040*, was generated. The deletion mutant was subjected to a series of physiological tests related to bacterial cell surface properties.

Biofilms are microbial communities that adhere to biotic or abiotic surfaces coated with self-produced extracellular polysaccharide materials (49). The adherence of cells and biofilm formation by the mutant were not significantly different from those for the wild-type strain when they were grown in nitrogen-enriched medium. However, the *A. vinelandii* Δ*Avin_16040* mutant strain demonstrated a significantly reduced biofilm formation on the

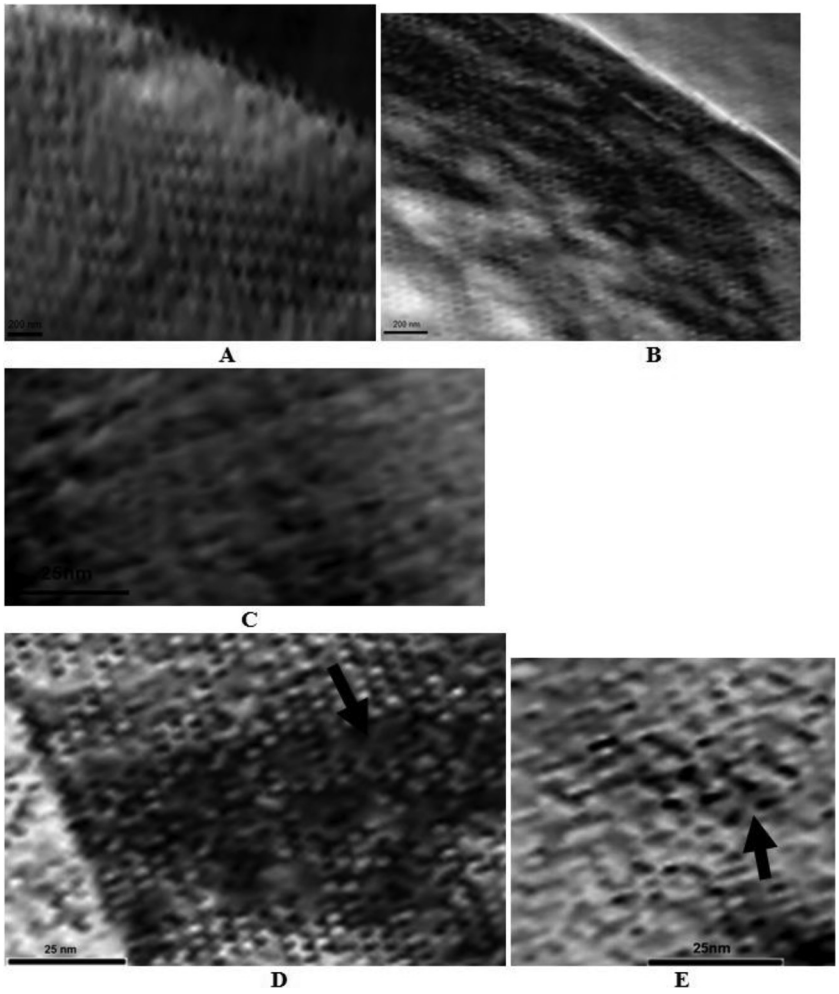

FIG 11 AFM images of cell surface topography of wild-type *A. vinelandii* ATCC 12837 (A), the Δ*Avin_16040* mutant (B), *E. coli* DH5α (C), colony *E. coli* DH5α(pJET1.2blunt:*Avin_16040*) (D), and root-attached *E. coli* DH5α(pJET1.2blunt:*Avin_16040*) (E). The images show increased S-protein density on the root-attached *E. coli* cell surface. Arrows indicate the S-protein monomer embedded on *E. coli* cell surface.

polystyrene surface compared to the wild type when grown in nitrogen-deficient medium. The effects of nitrogen on the cell membrane composition and cell membrane structure of *Azotobacter* were previously reported (50, 51). In addition, increased EPS production by an N_2-fixing *Rhizobium* sp. in growth medium supplied with various N sources compared to an N-free control has been reported (52).

Another property that has an effect on biofilm formation is the bacterial cell surface hydrophobicity. Cell surface hydrophobicity was determined by the ability of cells to adhere to hydrophobic hydrocarbon. In this study, a total loss of cell surface hydrophobicity was observed for the *A. vinelandii* Δ*Avin_16040* mutant strain compared to the wild type when both strains were grown in the N-free medium. The lost cell surface hydrophobicity indicated either a loss or reduced adhesion of bacterial cells to external surfaces. In *Staphylococcus aureus*, the cell surface hydrophobicity was shown to be determined by the bacterial surface proteins (53). By disrupting its cell surface proteins with proteolytic enzymes, *S. aureus* showed reduced bacterial cell surface hydrophobicity. Another factor that was in direct correlation with the cell surface hydrophobicity was autoaggregation of bacterial cells (53). In this study, reduced autoaggregation of Δ*Avin_16040* mutant cells compared to the wild type was observed.

The ability of the mutant to adhere to a biotic surface was also observed. The root attachment assay was performed to measure the ability to adhere to the plant root surface. Attachment of soil bacteria to plant cells is an important stage because it serves as the opening step required in plant-microbe interactions. This step is also necessary for the formation of microbial biofilms on plant roots (54, 55). The *A. vinelandii* Δ*Avin_16040* mutant demonstrated a significantly reduced root surface attachment compared to the wild type. Just like adhesion to the polystyrene (abiotic) surface, the difference was more significant when the adherence assay was performed in the N-free medium. This finding suggests that the hypothetical protein Avin_16040 is involved in the adherence of the bacterial cells to the plant root surface. The capacity for microbial attachment to plant cells is very important to the competitiveness of microbes to colonize plant roots.

Introduction of the *Avin_16040* gene into an *E. coli* DH5α host produced a morphological change in its customarily rod-shaped cells. Elongated filamentous cells and transparent "tube-like" morphologies were observed. The results were similar to a report

by Lederer et al. (56), who expressed the *Lysinibacillus sphaericus* JG-A12 S-layer-like protein SIIB gene in *E. coli* and observed filamentous cells with long, transparent, tube-like structures. The production of the heterologous S-layer protein possibly caused an alteration in cell morphology and a drastic change in the membrane property of the *E. coli* host.

Transmission electron micrographic (TEM) analysis of Δ*Avin_16040* mutant cells a revealed partial absence of their cell envelope as indicated by an incomplete border lining that enveloped the mutant cells. Enlarged views of the wild-type and mutant cells revealed a probable loss of the S-layer matrix in the mutant cells. The mutant strain appeared to develop a thick capsule-like layer of unknown identity. However, *A. vinelandii* is one of the bacterial species that produce both capsule and S-layer (57). Both components are important adhesion factors which contribute to the initial binding of bacterial cells to external surfaces for attachment (54). Structural characterizations of the tetragonal S-layer of *A. vinelandii* have been previously reported (35). The S-layer of *A. vinelandii* is an assembly of tetrameric structure located at the outermost surface of the bacterial cell (36). The organization consists of four identical subunits of a 60,000-molecular-weight protein (S protein), and the molecular weight of each tetrad unit was estimated to be 255,000. The assembly of the tetragonal surface array is induced by the divalent cations Ca^{2+} and Mg^{2+}.

Despite S-layer proteins being one of the most abundant cellular proteins of archaea and bacteria, observations on mutants lacking the bacterial S-layer proteins are scarce. AFM observation revealed the absence of the S-layer matrix on the Δ*Avin_16040* mutant cell surface. Surprisingly *E. coli* cells transformed with the full gene sequence of *Avin_16040* showed a series of regularly arranged monomer motifs on their surface. Moreover, the acquired monomer size of approximately 13 nm was like that reported for *A. vinelandii* (36). This evidence substantiates the possibility that the hypothetical protein Avin_16040 is the tetragonal S-layer protein of *A. vinelandii*. Intriguingly, the presence of the Avin_16040 protein in *E. coli* also enhanced its ability to adhere to the root surface. This raised the possibility of transferring the root-adhering property to a bacterial species that has high growth-promoting activity to enable it to exert maximum effects in its plant host.

In conclusion, we have shown that an interesting protein was present only when *A. vinelandii* cells were attached to the *O. sativa* root surface and that it was encoded by hypothetical gene *Avin_16040*. The proteins most similar to it are the bacterial S-layer proteins. The gene has been shown to be important for adherence, as shown by its induction when exposed to roots and the reduced adhesion activity of its mutant. An *E. coli* host of the *Avin_16040* gene showed enhanced adhesion to root surfaces, opening the prospect of enhancing root-adhesive properties of free-living plant-growth-promoting bacteria.

ACKNOWLEDGMENTS

This project was financially supported by the Malaysian Nuclear Agency and Universiti Sains Malaysia.

We thank Padiberas Nasional Berhad (Bernas) for courteously providing the *O. sativa* MR 219 seeds, Zahid Abdullah of the Malaysian Nuclear Agency for expert technical assistance on atomic force microscopy, Mohd Suhaimi Che Ani for help with electron microscopy, and Yam Hok Chai for generously providing technical advice on mutant analysis.

REFERENCES

1. **Sadoff HL.** 1975. Encystment and germination in Azotobacter vinelandii. Bacteriol Rev **39:**516–539.
2. **Rodelas B, González-López J, Pozo C, Salmerón V, Martínez-Toledo MV.** 1999. Response of faba bean (Vicia faba L.) to combined inoculation with Azotobacter and Rhizobium leguminosarum bv. viceae. Appl Soil Ecol **12:**51–59. http://dx.doi.org/10.1016/S0929-1393(98)00157-7.
3. **Kennedy C, Toukdarian A.** 1987. Genetics of azotobacters: applications to nitrogen fixation and related aspects of metabolism. Annu Rev Microbiol **41:**227–258. http://dx.doi.org/10.1146/annurev.mi.41.100187.001303.
4. **Gonzalez-Lopez J, Salmeron V, Martinez-Toledo MV, Ballesteros F, Ramos-Cormenzana A.** 1986. Production of auxins, gibberellins and cytokinins by Azotobacter vinelandii ATCC 12837 in chemically-defined media and dialysed soil media. Soil Biol Biochem **18:**119–120. http://dx.doi.org/10.1016/0038-0717(86)90115-X.
5. **Diaz-Barrera A, Soto E.** 2010. Biotechnological uses of Azotobacter vinelandii: current state, limits and prospects. Afr J Biotechnol **9:**5240–5250.
6. **Bais HP, Weir TL, Perry LG, Gilroy S, Vivanco JM.** 2006. The role of root exudates in rhizosphere interactions with plants and other organisms. Annu Rev Plant Biol **57:**233–266. http://dx.doi.org/10.1146/annurev.arplant.57.032905.105159.
7. **Setubal JC, dos Santos P, Goldman BS, Ertesvag H, Espin G, Rubio LM, Valla S, Almeida NF, Balasubramanian D, Cromes L, Curatti L, Du Z, Godsy E, Goodner B, Hellner-Burris K, Hernandez JA, Houmiel K, Imperial J, Kennedy C, Larson TJ, Latreille P, Ligon LS, Lu J, Maerk M, Miller NM, Norton S, O'Carroll IP, Paulsen I, Raulfs EC, Roemer R, Rosser J, Segura D, Slater S, Stricklin SL, Studholme DJ, Sun J, Viana CJ, Wallin E, Wang B, Wheeler C, Zhu H, Dean DR, Dixon R, Wood D.** 2009. Genome sequence of Azotobacter vinelandii, an obligate aerobe specialized to support diverse anaerobic metabolic processes. J Bacteriol **191:**4534–4545. http://dx.doi.org/10.1128/JB.00504-09.
8. **Brechenmacher L, Lei Z, Libault M, Findley S, Sugawara M, Sadowsky MJ, Sumner LW, Stacey G.** 2010. Soybean metabolites regulated in root hairs in response to the symbiotic bacterium Bradyrhizobium japonicum. Plant Physiol **153:**1808–1822. http://dx.doi.org/10.1104/pp.110.157800.
9. **Stacey G, Libault M, Brechenmacher L, Wan J, May GD.** 2006. Genetics and functional genomics of legume nodulation. Curr Opin Plant Biol **9:**110–121. http://dx.doi.org/10.1016/j.pbi.2006.01.005.
10. **Werner D.** 2001. Organic signals between plants and microorganisms, p 197–222. *In* Pinton R, Varanini Z, Nannipieri P (ed), The rhizosphere. Biochemistry and organic substances at the soil-plant interface. Marcel Dekker, New York, NY.
11. **Bestel-Corre G, Dumas-Gaudot E, Gianinazzi S.** 2004. Proteomics as a tool to monitor plant-microbe endosymbioses in the rhizosphere. Mycorrhiza **14:**1–10. http://dx.doi.org/10.1007/s00572-003-0280-3.
12. **Hauberg-Lotte L, Klingenberg H, Scharf C, Bohm M, Plessl J, Friedrich F, Volker U, Becker A, Reinhold-Hurek B.** 2012. Environmental factors affecting the expression of pilAB as well as the proteome and transcriptome of the grass endophyte Azoarcus sp. strain BH72. PLoS One **7:**e30421. http://dx.doi.org/10.1371/journal.pone.0030421.
13. **Muyzer G, de Waal EC, Uitterlinden AG.** 1993. Profiling of complex microbial populations by denaturing gradient gel electrophoresis analysis of polymerase chain reaction-amplified genes coding for 16S rRNA. Appl Environ Microbiol **59:**695–700.
14. **Ashby SF.** 1907. Some observations on the assimilation of atmospheric nitrogen by a free living soil organism, Azotobacter chroococcum of Beijerinck. J Agric Sci **2:**35–51. http://dx.doi.org/10.1017/S0021859600000988.
15. **Murashige T, Skoog F.** 1962. A revised medium for rapid growth and bio-assays with tobacco tissue cultures. Physiol Plant **15:**473–497. http://dx.doi.org/10.1111/j.1399-3054.1962.tb08052.x.
16. **Davison J, Heusterspreute M, Chevalier N, Ha-Thi V, Brunel F.** 1987. Vectors with restriction site banks. V. pJRD215, a wide-host-range cosmid vector with multiple cloning sites. Gene **51:**275–280.
17. **Anand RD, Sertil O, Lowry CV.** 2004. Restriction digestion monitors facilitate plasmid construction and PCR cloning. Biotechniques **36:**982–985.
18. **Page WJ, Sadoff HL.** 1976. Control of transformation competence in Azotobacter vinelandii by nitrogen catabolite derepression. J Bacteriol **125:**1088–1095.

19. **Maldonado R, Jimenez J, Casadesus J.** 1994. Changes of ploidy during the Azotobacter vinelandii growth cycle. J Bacteriol **176:**3911–3919.
20. **Milton DL, O'Toole R, Horstedt P, Wolf-Watz H.** 1996. Flagellin A is essential for the virulence of Vibrio anguillarum. J Bacteriol **178:**1310–1319.
21. **Blomfield IC, McClain MS, Eisenstein BI.** 1991. Type 1 fimbriae mutants of Escherichia coli K12: characterization of recognized afimbriate strains and construction of new fim deletion mutants. Mol Microbiol **5:**1439–1445. http://dx.doi.org/10.1111/j.1365-2958.1991.tb00790.x.
22. **Ullah H, Ullah I, Jadoon SA, Rashid H.** 2007. Tissue culture techniques for callus induction in rice. Sarhad J Agric **23:**81–86.
23. **Sambrook J, Russell DW.** 2001. Molecular cloning: a laboratory manual, 3rd ed. Cold Spring Harbor Laboratory Press, Cold Spring Harbor, NY.
24. **McGregor E, Kempster L, Wait R, Gosling M, Dunn MJ, Powell JT.** 2004. F-actin capping (CapZ) and other contractile saphenous vein smooth muscle proteins are altered by hemodynamic stress: a proteonomic approach. Mol Cell Proteomics **3:**115–124.
25. **Perkins DN, Pappin DJ, Creasy DM, Cottrell JS.** 1999. Probability-based protein identification by searching sequence databases using mass spectrometry data. Electrophoresis **20:**3551–3567. http://dx.doi.org/10.1002/(SICI)1522-2683(19991201)20:18<3551::AID-ELPS3551>3.0.CO;2-2.
26. **Schmittgen TD, Livak KJ.** 2008. Analyzing real-time PCR data by the comparative C_T method. Nat Protoc **3:**1101–1108. http://dx.doi.org/10.1038/nprot.2008.73.
27. **Glauert AM.** 1975. Practical methods in electron microscopy, vol 3. Fixation, dehydration and embedding of biological specimens. North-Holland Publishing Company, Amsterdam, The Netherlands.
28. **O'Toole GA, Kolter R.** 1998. Flagellar and twitching motility are necessary for Pseudomonas aeruginosa biofilm development. Mol Microbiol **30:**295–304. http://dx.doi.org/10.1046/j.1365-2958.1998.01062.x.
29. **Škvarla J, Kupka D, Turčániová L.** 2002. A complementary study of hydrophobicity and surface charge of Thiobacillus ferrooxidans. The effect of ionic surfactants. Acta Montanistica Slovaca Ročník **7:**85–88.
30. **Albareda M, Dardanelli MS, Sousa C, Megias M, Temprano F, Rodriguez-Navarro DN.** 2006. Factors affecting the attachment of rhizospheric bacteria to bean and soybean roots. FEMS Microbiol Lett **259:**67–73. http://dx.doi.org/10.1111/j.1574-6968.2006.00244.x.
31. **Robledo M, Rivera L, Jimenez-Zurdo JI, Rivas R, Dazzo F, Velazquez E, Martinez-Molina E, Hirsch AM, Mateos PF.** 2012. Role of Rhizobium endoglucanase CelC2 in cellulose biosynthesis and biofilm formation on plant roots and abiotic surfaces. Microb Cell Fact **11:**125. http://dx.doi.org/10.1186/1475-2859-11-125.
32. **Thompson JD, Higgins DG, Gibson TJ.** 1994. CLUSTAL W: improving the sensitivity of progressive multiple sequence alignment through sequence weighting, position-specific gap penalties and weight matrix choice. Nucleic Acids Res **22:**4673–4680. http://dx.doi.org/10.1093/nar/22.22.4673.
33. **Tusnady GE, Simon I.** 2001. The HMMTOP transmembrane topology prediction server. Bioinformatics **17:**849–850. http://dx.doi.org/10.1093/bioinformatics/17.9.849.
34. **Moller S, Croning MD, Apweiler R.** 2001. Evaluation of methods for the prediction of membrane spanning regions. Bioinformatics **17:**646–653. http://dx.doi.org/10.1093/bioinformatics/17.7.646.
35. **Bingle WH, Engelhardt H, Page WJ, Baumeister W.** 1987. Three-dimensional structure of the regular tetragonal surface layer of Azotobacter vinelandii. J Bacteriol **169:**5008–5015.
36. **Bingle WH, Whippey PW, Doran JL, Murray RG, Page WJ.** 1987. Structure of the Azotobacter vinelandii surface layer. J Bacteriol **169:**802–810.
37. **Dooley JS, Engelhardt H, Baumeister W, Kay WW, Trust TJ.** 1989. Three-dimensional structure of an open form of the surface layer from the fish pathogen Aeromonas salmonicida. J Bacteriol **171:**190–197.
38. **Dooley JS, McCubbin WD, Kay CM, Trust TJ.** 1988. Isolation and biochemical characterization of the S-layer protein from a pathogenic Aeromonas hydrophila strain. J Bacteriol **170:**2631–2638.
39. **Austin JW, Stewart M, Murray RG.** 1990. Structural and chemical characterization of the S layer of a Pseudomonas-like bacterium. J Bacteriol **172:**808–817.
40. **Sara M, Sleytr UB.** 2000. S-layer proteins. J Bacteriol **182:**859–868. http://dx.doi.org/10.1128/JB.182.4.859-868.2000.
41. **Sleytr UB.** 1978. Regular arrays of macromolecules on bacterial cell walls: structure, chemistry, assembly, and function. Int Rev Cytol **53:**1–62. http://dx.doi.org/10.1016/S0074-7696(08)62240-8.
42. **Sleytr UB, Sara M, Messner P, Pum D.** 1994. Two-dimensional protein crystals (S-layers): fundamentals and applications. J Cell Biochem **56:**171–176. http://dx.doi.org/10.1002/jcb.240560209.
43. **Sleytr UB, Messner P, Pum D, Sara M.** 1993. Crystalline bacterial cell surface layers. Mol Microbiol **10:**911–916. http://dx.doi.org/10.1111/j.1365-2958.1993.tb00962.x.
44. **Rohlin L, Leon DR, Kim U, Loo JA, Ogorzalek Loo RR, Gunsalus RP.** 2012. Identification of the major expressed S-layer and cell surface-layer-related proteins in the model methanogenic archaea: Methanosarcina barkeri Fusaro and Methanosarcina acetivorans C2A. Archaea **2012:**873589. http://dx.doi.org/10.1155/2012/873589.
45. **Dohm N, Petri A, Schlander M, Schlott B, Konig H, Claus H.** 2011. Molecular and biochemical properties of the S-layer protein from the wine bacterium Lactobacillus hilgardii B706. Arch Microbiol **193:**251–261. http://dx.doi.org/10.1007/s00203-010-0670-9.
46. **Jarrell KF, Jones GM, Kandiba L, Nair DB, Eichler J.** 2010. S-layer glycoproteins and flagellins: reporters of archaeal posttranslational modifications. Archaea **2010:**612948. http://dx.doi.org/10.1155/2010/612948.
47. **Avall-Jaaskelainen S, Hynonen U, Ilk N, Pum D, Sleytr UB, Palva A.** 2008. Identification and characterization of domains responsible for self-assembly and cell wall binding of the surface layer protein of Lactobacillus brevis ATCC 8287. BMC Microbiol **8:**165. http://dx.doi.org/10.1186/1471-2180-8-165.
48. **Merrigan MM, Venugopal A, Roxas JL, Anwar F, Mallozzi MJ, Roxas BA, Gerding DN, Viswanathan VK, Vedantam G.** 2013. Surface-layer protein A (SlpA) is a major contributor to host-cell adherence of Clostridium difficile. PLoS One **8:**e78404. http://dx.doi.org/10.1371/journal.pone.0078404.
49. **Olson ME, Ceri H, Morck DW, Buret AG, Read RR.** 2002. Biofilm bacteria: formation and comparative susceptibility to antibiotics. Can J Vet Res **66:**86–92.
50. **Marcus L, Kaneshiro T.** 1972. Lipid composition of Azotobacter vinelandii in which the internal membrane network is induced or repressed. Biochim Biophys Acta **288:**296–303. http://dx.doi.org/10.1016/0005-2736(72)90250-7.
51. **Oppenheim J, Marcus L.** 1970. Correlation of ultrastructure in Azotobacter vinelandii with nitrogen source for growth. J Bacteriol **101:**286–291.
52. **Mukherjee S, Ghosh S, Sadhu S, Ghosh P, Maiti TK.** 2011. Extracellular polysaccharide production by a Rhizobium sp isolated from legume herb Crotalaria saltiana Andr. Indian J Biotechnol **10:**340–345.
53. **Ljungh A, Hjerten S, Wadstrom T.** 1985. High surface hydrophobicity of autoaggregating Staphylococcus aureus strains isolated from human infections studied with the salt aggregation test. Infect Immun **47:**522–526.
54. **Rodriguez-Navarro DN, Dardanelli MS, Ruiz-Sainz JE.** 2007. Attachment of bacteria to the roots of higher plants. FEMS Microbiol Lett **272:**127–136. http://dx.doi.org/10.1111/j.1574-6968.2007.00761.x.
55. **Smit G, Swart S, Lugtenberg BJ, Kijne JW.** 1992. Molecular mechanisms of attachment of Rhizobium bacteria to plant roots. Mol Microbiol **6:**2897–2903. http://dx.doi.org/10.1111/j.1365-2958.1992.tb01748.x.
56. **Lederer FL, Gunther TJ, Flemming K, Raff J, Fahmy K, Springer A, Pollmann K.** 2010. Heterologous expression of the surface-layer-like protein SIIB induces the formation of long filaments of *Escherichia coli* consisting of protein-stabilized outer membrane. Microbiology **156:**3584–3595. http://dx.doi.org/10.1099/mic.0.040808-0.
57. **Mesnage S, Tosi-Couture E, Mock M, Fouet A.** 1999. The S-layer homology domain as a means for anchoring heterologous proteins on the cell surface of Bacillus anthracis. J Appl Microbiol **87:**256–260. http://dx.doi.org/10.1046/j.1365-2672.1999.00880.x.